

A Second Order Non-smooth Variational Model for Restoring Manifold-valued Images

Ronny Bergmann*

University of Kaiserslautern

September 30, 2015

First Applied Mathematics Symposium Münster
Variational Methods for Dynamic Inverse Problems and Imaging,
Münster

* joint work with M. Bačák (MPI MIS Leipzig),
G. Steidl (U Kaiserslautern), A. Weinmann (TU Munich)



Contents

- 1 Introduction
- 2 Second Order Differences on Manifolds
- 3 Proximal Mappings and the Cyclic Proximal Point Algorithm
- 4 Examples
- 5 Conclusion

- 1 Introduction
- 2 Second Order Differences on Manifolds
- 3 Proximal Mappings and the Cyclic Proximal Point Algorithm
- 4 Examples
- 5 Conclusion

Restoring Images: Denoising and Inpainting

Introducing discrete total variation models for real valued data.

- given noisy image $f: \mathcal{V} \rightarrow \mathbb{R}$, $\mathcal{V} \subseteq \mathcal{G} = \{1, \dots, N\} \times \{1, \dots, M\}$
- reconstruct original image $u_0: \mathcal{G} \rightarrow \mathbb{R}$
- pixel from $\mathcal{G} \setminus \mathcal{V}$ have to be inpainted
- approach: Minimize variational model

$$\mathcal{E}(u) := \underbrace{F(f, u)}_{\text{data term}} + \underbrace{\alpha R(u)}_{\text{regularization term}}, \quad \alpha > 0$$

- first order models (total variation, TV) [Rudin, Osher, Fatemi, 1992]
 - isotropic model with discrete gradient $|\nabla u|$: $R_{\text{iso}}(u) := \sum_{i,j} |\nabla u|$
 - anisotropic model: $R_{\text{aniso}}(u) := \sum_{i,j} (|u_{i+1,j} - u_{i,j}| + |u_{i,j+1} - u_{i,j}|)$
 - edge preserving
- several higher order variational models avoid **stair causing-effect**

[Chambolle, Lions, 1997; Setzer, Steidl, 2008; Bredies, Kunisch, Pock, 2010; Papafitsoros, Schönlieb, 2014]

Riemannian Manifolds

...which we want to apply in different spaces

Here: Images with pixel values in a Riemannian manifold \mathcal{M}

Goal: Second Order Model for images $f: \mathcal{V} \rightarrow \mathcal{M}$

Applications with manifold-valued images

\mathbb{S}^1 InSAR, HSI(HSV) color space, phase space

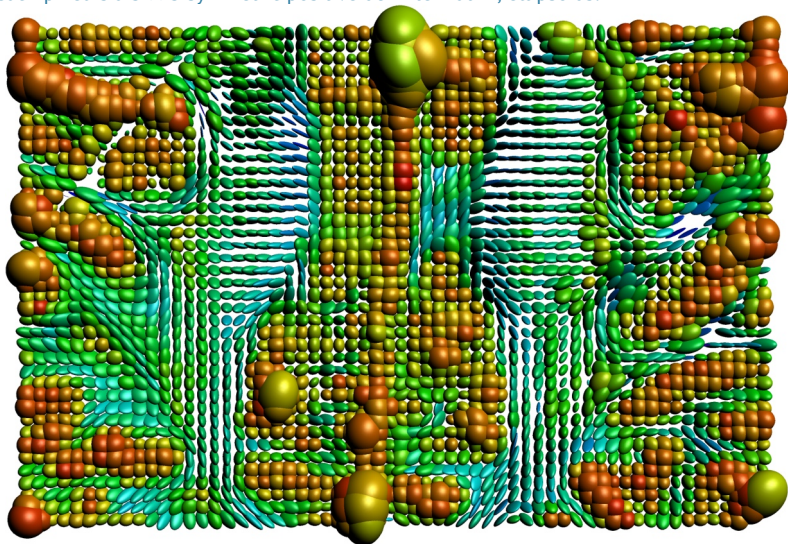
\mathbb{S}^2 directions, chromaticity-brightness colorspace

$SO(3)$ orientations, electron backscattered diffraction

$\mathcal{P}(s)$ DT-MRI, covariance matrices

Symmetric Positive Definite Matrices: $x^T A x > 0$

$\mathcal{P}(3)$: each pixel is a 3×3 symmetric positive definite matrix, ellipsoids: $x^T A x = 1$



1 Introduction

2 Second Order Differences on Manifolds

3 Proximal Mappings and the Cyclic Proximal Point Algorithm

4 Examples

5 Conclusion

First and Second Order Differences

Let's restrict ourselves to signals for now...

$$\mathcal{G} = \{1, \dots, N\}, \mathcal{V} \subset \mathcal{G}$$

On \mathbb{R}^n

- line $\gamma(t) = x + t(y - x)$
- distance $\|x - y\|_2$
- first order model

$$\sum_{i \in \mathcal{V}} \|f_i - u_i\|_2^2 + \alpha \sum_{i \in \mathcal{G} \setminus \{N\}} \|u_i - u_{i+1}\|_2$$

Riemannian manifold \mathcal{M}

- geodesic path $\gamma_{\widehat{x,z}}(t)$
- geodesic distance $d: \mathcal{M} \times \mathcal{M} \rightarrow \mathbb{R}_{\geq 0}$
- first order model

$$\sum_{i \in \mathcal{V}} d(f_i, u_i)^2 + \alpha \sum_{i \in \mathcal{G} \setminus \{N\}} d(u_i, u_{i+1})$$

First and Second Order Differences

Let's restrict ourselves to signals for now...

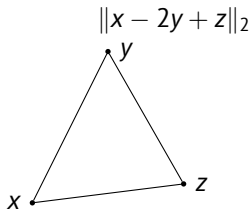
$$\mathcal{G} = \{1, \dots, N\}, \mathcal{V} \subset \mathcal{G}$$

On \mathbb{R}^n

- line $\gamma(t) = x + t(y - x)$
- distance $\|x - y\|_2$
- first order model

$$\sum_{i \in \mathcal{V}} \|f_i - u_i\|_2^2 + \alpha \sum_{i \in \mathcal{G} \setminus \{N\}} \|u_i - u_{i+1}\|_2$$

- second order difference

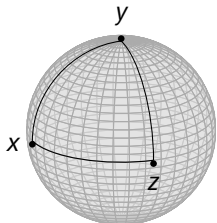


Riemannian manifold \mathcal{M}

- geodesic path $\gamma_{x,z}(t)$
- geodesic distance $d: \mathcal{M} \times \mathcal{M} \rightarrow \mathbb{R}_{\geq 0}$
- first order model

$$\sum_{i \in \mathcal{V}} d(f_i, u_i)^2 + \alpha \sum_{i \in \mathcal{G} \setminus \{N\}} d(u_i, u_{i+1})$$

- How to model that on \mathcal{M} ?



$$\mathcal{M} = \mathbb{S}^2$$

First and Second Order Differences

Let's restrict ourselves to signals for now...

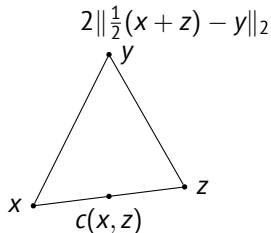
$$\mathcal{G} = \{1, \dots, N\}, \mathcal{V} \subset \mathcal{G}$$

On \mathbb{R}^n

- line $\gamma(t) = x + t(y - x)$
- distance $\|x - y\|_2$
- first order model

$$\sum_{i \in \mathcal{V}} \|f_i - u_i\|_2^2 + \alpha \sum_{i \in \mathcal{G} \setminus \{N\}} \|u_i - u_{i+1}\|_2$$

- second order difference

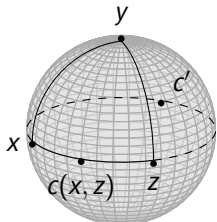


Riemannian manifold \mathcal{M}

- geodesic path $\gamma_{x,z}(t)$
- geodesic distance $d: \mathcal{M} \times \mathcal{M} \rightarrow \mathbb{R}_{\geq 0}$
- first order model

$$\sum_{i \in \mathcal{V}} d(f_i, u_i)^2 + \alpha \sum_{i \in \mathcal{G} \setminus \{N\}} d(u_i, u_{i+1})$$

- **idea:** mid point formulation



$$\mathcal{M} = \mathbb{S}^2$$

First and Second Order Differences

Let's restrict ourselves to signals for now...

$$\mathcal{G} = \{1, \dots, N\}, \mathcal{V} \subset \mathcal{G}$$

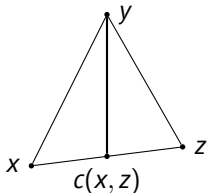
On \mathbb{R}^n

- line $\gamma(t) = x + t(y - x)$
- distance $\|x - y\|_2$
- first order model

$$\sum_{i \in \mathcal{V}} \|f_i - u_i\|_2^2 + \alpha \sum_{i \in \mathcal{G} \setminus \{N\}} \|u_i - u_{i+1}\|_2$$

- second order difference

$2\|c(x, z) - y\|_2$, $c(x, y)$: mid point

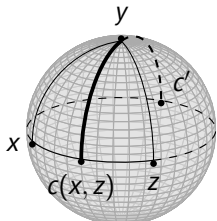


Riemannian manifold \mathcal{M}

- geodesic path $\gamma_{x,z}(t)$
- geodesic distance $d: \mathcal{M} \times \mathcal{M} \rightarrow \mathbb{R}_{\geq 0}$
- first order model

$$\sum_{i \in \mathcal{V}} d(f_i, u_i)^2 + \alpha \sum_{i \in \mathcal{G} \setminus \{N\}} d(u_i, u_{i+1})$$

- **idea:** mid point formulation



$$\mathcal{M} = \mathbb{S}^2$$

A Second Order TV-type Model

Mid points between $x, z \in \mathcal{M}$:

$$\mathcal{C}_{x,z} := \left\{ c \in \mathcal{M} : c = \gamma_{\widehat{x,z}}\left(\frac{T}{2}\right) \text{ for any geodesic } \gamma_{\widehat{x,z}}, T := \mathcal{L}(\gamma_{\widehat{x,z}}) \right\}$$

The **Absolute Second Order Difference**:

$$d_2(x, y, z) := \min_{c \in \mathcal{C}_{x,z}} d(c, y), \quad x, y, z \in \mathcal{M}.$$

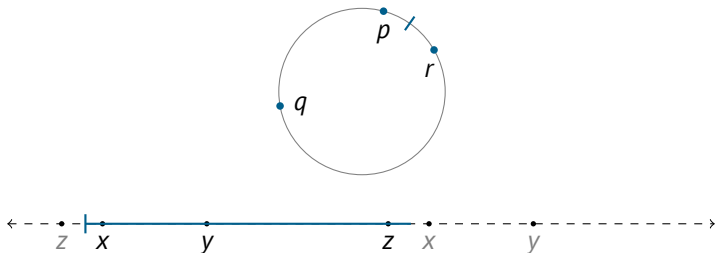
⇒ **Second Order TV-type Model** for \mathcal{M} -valued signals f

$$\mathcal{E}(u) := \sum_{i \in \mathcal{V}} d(f_i, u_i)^2 + \alpha \sum_{i \in \mathcal{G} \setminus \{N\}} d(u_i, u_{i+1}) + \beta \sum_{i \in \mathcal{G} \setminus \{1, N\}} d_2(u_{i-1}, u_i, u_{i+1})$$

Example: the Circle \mathbb{S}^1

Cyclic data: $p, q, r \in \mathbb{S}^1 := \{s \in \mathbb{R}^2 : \|s\|_2 = 1\} \iff x, y, z \in [-\pi, \pi)$

$d_2(x, y, z)$: Several unwrappings

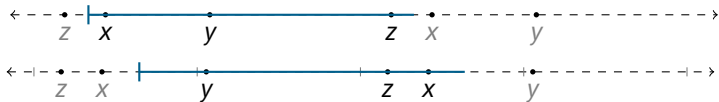
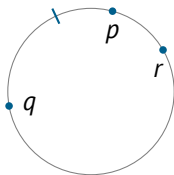


$$|x - 2y + z|$$

Example: the Circle \mathbb{S}^1

Cyclic data: $p, q, r \in \mathbb{S}^1 := \{s \in \mathbb{R}^2 : \|s\|_2 = 1\} \iff x, y, z \in [-\pi, \pi]$

$d_2(x, y, z)$: Several unwrappings

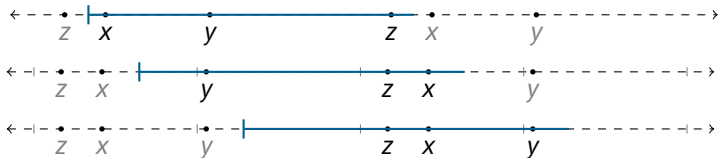
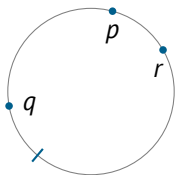


$$|x - 2y + z|$$

Example: the Circle \mathbb{S}^1

Cyclic data: $p, q, r \in \mathbb{S}^1 := \{s \in \mathbb{R}^2 : \|s\|_2 = 1\} \iff x, y, z \in [-\pi, \pi)$

$d_2(x, y, z)$: Several unwrappings

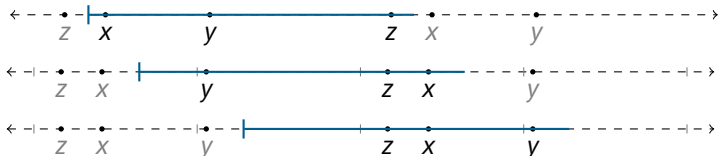
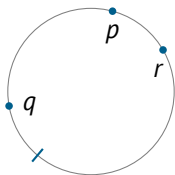


$$|x - 2y + z|$$

Example: the Circle \mathbb{S}^1

Cyclic data: $p, q, r \in \mathbb{S}^1 := \{s \in \mathbb{R}^2 : \|s\|_2 = 1\} \iff x, y, z \in [-\pi, \pi)$

$d_2(x, y, z)$: Minimize over all unwrappings



$$d_2(x, y, z) := \min_{\mu \in \mathbb{R}} |(x + \mu) - 2(y + \mu) + (z + \mu)| = |(x - 2y + z)_{2\pi}|$$

- 1 Introduction
- 2 Second Order Differences on Manifolds
- 3 Proximal Mappings and the Cyclic Proximal Point Algorithm**
- 4 Examples
- 5 Conclusion

Proximal Mappings

Proximal algorithms are standard tool for solving non-smooth, constrained minimization problems.

To compute a minimizer of $\mathcal{E}(u)$ we need **proximal mappings**

For a proper, closed, convex function $\varphi: \mathbb{R}^n \rightarrow (-\infty, +\infty]$ and $\lambda > 0$ the **proximal mapping** is defined by

[Moreau, 1965; Rockafellar, 1976]

$$\text{prox}_{\lambda\varphi}(g) := \arg \min_{u \in \mathbb{R}^n} \frac{1}{2} \|u - g\|_2^2 + \lambda\varphi(u).$$

For a function $\varphi: \mathcal{M}^n \rightarrow (-\infty, +\infty]$ and $\lambda > 0$ the **proximal mapping** is defined by

[Ferreira, Oliveira, 2002]

$$\text{prox}_{\lambda\varphi}(g) := \arg \min_{u \in \mathcal{M}^n} \frac{1}{2} \sum_{i=1}^n d(u_i, g_i)^2 + \lambda\varphi(u).$$

Note: For a minimizer u^* of φ it holds $\text{prox}_{\lambda\varphi}(u^*) = u^*$.

The Cyclic Proximal Point Algorithm

Splitting large φ into smaller problems.

To find $\arg \min_x \varphi(x)$ use Picard iteration: **Proximal Point Algorithm**

$$x^{(k)} = \text{prox}_{\lambda\varphi}(x^{(k-1)}), \quad k > 0$$

\Rightarrow fast evaluation of $\text{prox}_{\lambda\varphi}$ needed

For $\varphi = \sum_{l=1}^c \varphi_l$ use **Cyclic Proximal Point Algorithm (CPPA)**

[Bertsekas, 2011]

$$x^{(k+\frac{l+1}{c})} = \text{prox}_{\lambda_k\varphi_l}(x^{(k+\frac{l}{c})}), \quad i = 0, \dots, c-1, k > 0$$

For **real-valued data**:

Converges to a minimizer if $\{\lambda_k\} \in \ell_2(\mathbb{Z}) \setminus \ell_1(\mathbb{Z})$.

Minimizing the Second Order Model

Applying the CPPA to our model on manifolds.

To minimize

$$\mathcal{E}(u) := \sum_{i \in \mathcal{V}} d(f_i, u_i)^2 + \alpha \sum_{i \in \mathcal{G} \setminus \{N\}} d(u_i, u_{i+1}) + \beta \sum_{i \in \mathcal{G} \setminus \{1, N\}} d_2(u_{i-1}, u_i, u_{i+1})$$

take each summand as one φ_l in the CPPA.

For the involved proximal maps we have

- $\varphi(u_i) = d(f_i, u_i)^2$, analytical solution [Ferreira, Oliveira, 2002]
- $\varphi(u_i, u_{i+1}) = d(u_i, u_{i+1})$, analytical solution [Weinmann, Storath, Demaret, 2014]
- $\varphi(u_{i-1}, u_i, u_{i+1}) = d_2(u_{i-1}, u_i, u_{i+1})$
 - analytical solution for \mathbb{S}^1 [B., Laus, Steidl, Weinmann, 2014]
 - numerical solution otherwise [Bačák, B., Steidl, Weinmann, 2015]

Proximal Mapping of a Second Order Difference on \mathcal{M}

To compute

$$\text{prox}_{\lambda d_2}(g) = \arg \min_{u \in \mathcal{M}^3} \left\{ \frac{1}{2} \sum_{i=1}^3 d(u_i, g_i)^2 + \lambda d_2(u_1, u_2, u_3) \right\}$$

(sub)gradient descent method requires gradient of $d_2(x, y, z) = d(c(x, z), y)$

$$\nabla_{\mathcal{M}^3} d_2 = (\nabla_{\mathcal{M}} d_2(\cdot, y, z), \nabla_{\mathcal{M}} d_2(x, \cdot, z), \nabla_{\mathcal{M}} d_2(x, y, \cdot))^T.$$

For $y \neq c(x, z)$ and an ONB $\{\xi_1, \dots, \xi_n\}$ of $T_x \mathcal{M}$

- $\nabla_{\mathcal{M}} d_2(x, \cdot, z)(y) = \frac{\log_y c(x, z)}{\|\log_y c(x, z)\|_y} \in T_y \mathcal{M}$
- $\nabla_{\mathcal{M}} d_2(\cdot, y, z)$ by chain rule

$$\nabla_{\mathcal{M}} d_2(\cdot, y, z)(x) = \sum_{k=1}^n \left\langle \frac{\log_{c(x)} y}{\|\log_{c(x)} y\|_{c(x)}}, D_x c[\xi_k] \right\rangle_{c(x)}, \quad \xi_k \in T_x \mathcal{M}.$$

Proximal Mapping of a Second Order Difference on \mathcal{M}

To compute

$$\text{prox}_{\lambda d_2}(g) = \arg \min_{u \in \mathcal{M}^3} \left\{ \frac{1}{2} \sum_{i=1}^3 d(u_i, g_i)^2 + \lambda d_2(u_1, u_2, u_3) \right\}$$

(sub)gradient descent method requires gradient of $d_2(x, y, z) = d(c(x, z), y)$

$$\nabla_{\mathcal{M}^3} d_2 = (\nabla_{\mathcal{M}} d_2(\cdot, y, z), \nabla_{\mathcal{M}} d_2(x, \cdot, z), \nabla_{\mathcal{M}} d_2(x, y, \cdot))^T.$$

For $y \neq c(x, z)$ and an ONB $\{\xi_1, \dots, \xi_n\}$ of $T_x \mathcal{M}$

- $\nabla_{\mathcal{M}} d_2(x, \cdot, z)(y) = \frac{\log_y c(x, z)}{\|\log_y c(x, z)\|_y} \in T_y \mathcal{M}$
- $\nabla_{\mathcal{M}} d_2(\cdot, y, z)$ by chain rule

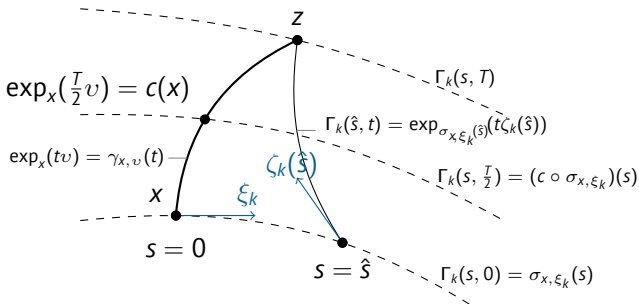
$$\nabla_{\mathcal{M}} d_2(\cdot, y, z)(x) = \sum_{k=1}^n \left\langle \frac{\log_{c(x)} y}{\|\log_{c(x)} y\|_{c(x)}}, D_x c[\xi_k] \right\rangle_{c(x)}, \quad \xi_k \in T_x \mathcal{M}.$$

Geodesic Variation

How do small changes in x affect the geodesic?

- $\sigma_{x, \xi_k}(s)$, $k = 1, \dots, n$, $s \in (-\varepsilon, \varepsilon)$:
curve starting in $\sigma_{x, \xi_k}(0) = x$ with direction $\sigma'_{x, \xi_k}(0) = \xi_k$
 - $\zeta_k(s)$: direction in $\sigma_{x, \xi_k}(s)$ towards z .
- ⇒ geodesic variation of the geodesic $\gamma_{x, z}$

$$\Gamma_k(s, t) := \exp_{\sigma_{x, \xi_k}(s)}(t\zeta_k(s)), \quad s \in (-\varepsilon, \varepsilon), \quad t \in [0, T], \quad T = d(x, z)$$



Jacobi Fields

Indicate directions of change along the geodesic and rephrase computation of the gradient to...

The Jacobi field J_k , $k = 1, \dots, n$, along $\gamma_{\widehat{x}, \widehat{z}}$ is defined by

$$J_k(t) := \frac{\partial}{\partial s} \Gamma_k(s, t) \Big|_{s=0}, \quad t \in [0, T]$$

Lemma

$$D_x c[\xi_k] = J_k\left(\frac{T}{2}\right)$$

Lemma

A Jacobi field J_k fulfills the System of ODEs

$$\frac{D^2}{dt^2} J_k + R(J_k, \dot{\gamma}_{\widehat{x}, \widehat{z}}) \dot{\gamma}_{\widehat{x}, \widehat{z}} = 0, \quad J_k(0) = \xi_k, \quad J_k(T) = 0$$

with the Riemannian curvature tensor $R: TM \times TM \times TM \rightarrow TM$.

Riemannian Symmetric Spaces

At least in beautiful Spaces we can solve the system of ODEs

- For every $x \in \mathcal{M}$ exists an isometry s_x on \mathcal{M} , i.e.

$$s_x(x) = x, D_x s[\xi] = -\xi, \quad \text{for all } \xi \in T_x \mathcal{M}$$

- covariant derivative

$$\nabla R = 0$$

⇒ the system of ODEs simplifies to a **linear system of ODEs with constant coefficients**

- Examples of symmetric spaces
 - Spheres \mathbb{S}^n
 - Hyperbolic Spaces
 - positive definite matrices $\mathcal{P}(s)$
 - Grasmannians

Riemannian symmetric spaces are the most beautiful and most important Riemannian manifolds.

(J.-H. Eschenburg, 1997)

The Derivative $D_x c[\xi_k]$ in Symmetric Spaces

Finally we are able to evaluate the Jacobi field at the mid point $T/2$

With parallel transport of an orthonormal frame $\{\Theta_1(t), \dots, \Theta_n(t)\}$, i.e.

$$J_k(t) = \sum_{i=1}^n a_{k,i}(t) \Theta_i(t).$$

and a specific ONB $\{\xi_1, \dots, \xi_n\}$ at $t = 0$ and κ_i “characterize curvature”

Corollary

With $T = d(x, z)$ we have for $k = 1, \dots, n$

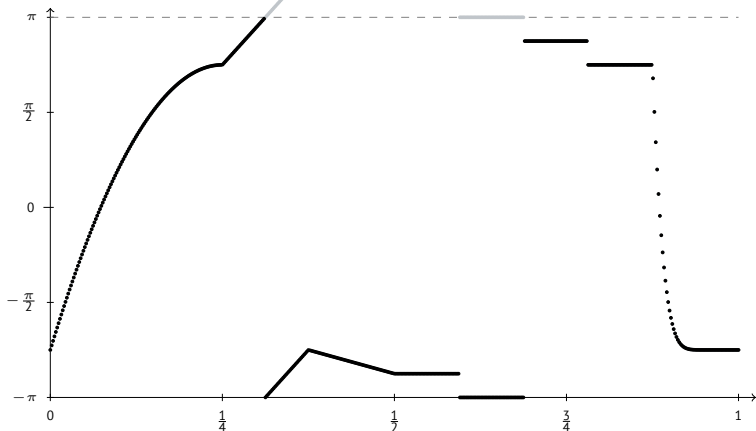
$$D_x c[\xi_k] = J_k\left(\frac{T}{2}\right) = \begin{cases} \frac{\sinh\left(\sqrt{-\kappa_k} \frac{T}{2}\right)}{\sinh(\sqrt{-\kappa_k} T)} \Theta_k\left(\frac{T}{2}\right), & \text{if } \kappa_k < 0, \\ \frac{\sin\left(\sqrt{\kappa_k} \frac{T}{2}\right)}{\sin(\sqrt{\kappa_k} T)} \Theta_k\left(\frac{T}{2}\right), & \text{if } \kappa_k > 0, \\ \frac{1}{2} \Theta_k\left(\frac{T}{2}\right), & \text{if } \kappa_k = 0. \end{cases}$$

⇒ Gradient descent to approximate the Proximal Mapping of the second order difference on a manifold.

- 1 Introduction
- 2 Second Order Differences on Manifolds
- 3 Proximal Mappings and the Cyclic Proximal Point Algorithm
- 4 Examples**
- 5 Conclusion

A Signal of Cyclic Data

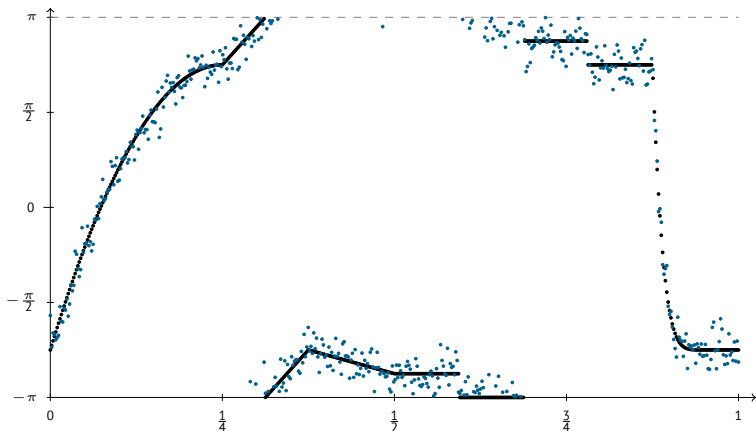
Noising a phase valued signal.



- function $f: [0, 1] \rightarrow \mathbb{S}^1$ sampled to obtain data $f_o = (f_{o,i})_{i=1}^{500}$
- f could be a wrapped version of the gray plot, hence
- jumps $> \pi$ at $\frac{5}{16}$ and $\frac{11}{16}$ are due to the representation system

A Signal of Cyclic Data

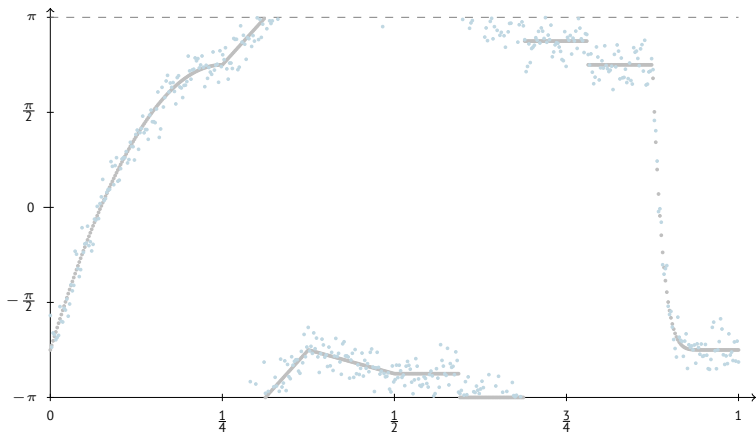
Noising a phase valued signal.



- function $f: [0, 1] \rightarrow \mathbb{S}^1$ sampled to obtain data $f_0 = (f_{0,i})_{i=1}^{500}$
- adding wrapped Gaussian noise, $\sigma = 0.2$
- noisy data $f_n = (f_0 + \eta)_{2\pi}$

A Signal of Cyclic Data

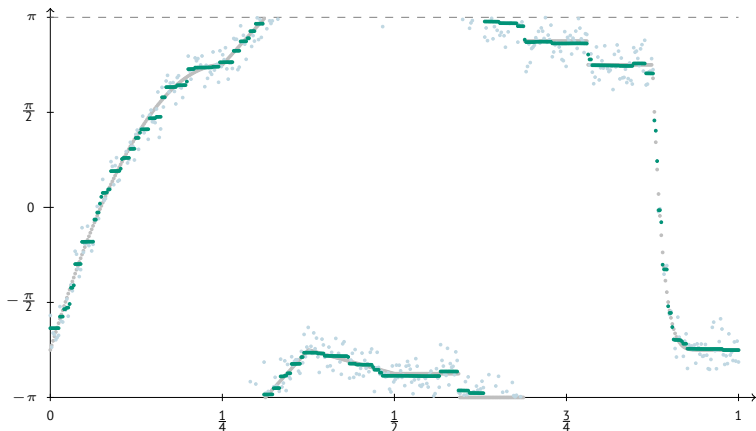
Noising a phase valued signal.



■ comparison of f_0 & f_n with

A Signal of Cyclic Data

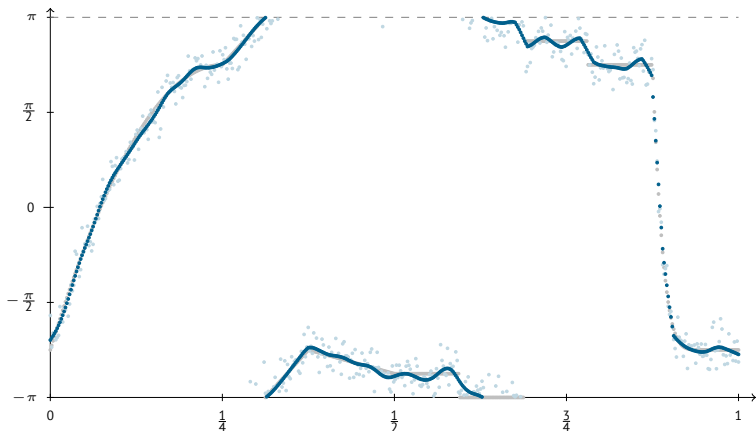
Denoising a phase valued signal.



- comparison of f_0 & f_n with f_1
- denoising TV_1 ($\alpha = \frac{3}{4}, \beta = 0$)
- but: stair casing

A Signal of Cyclic Data

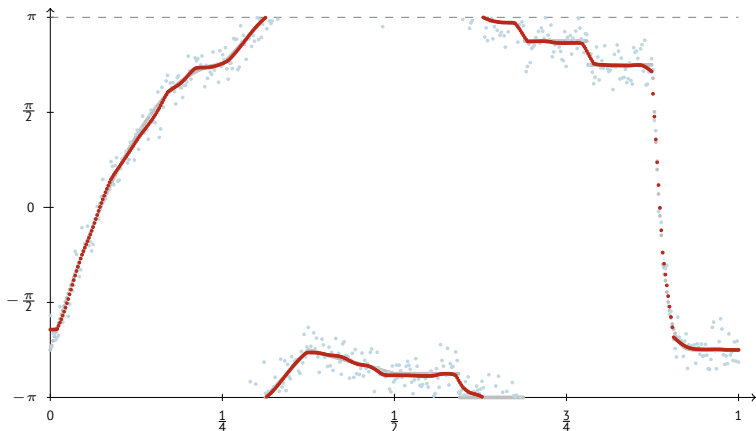
Denoising a phase valued signal.



- comparison of f_0 & f_n with f_2
- denoising TV_2 ($\alpha = 0, \beta = \frac{3}{2}$)
- but: no plateaus

A Signal of Cyclic Data

Denoising a phase valued signal.



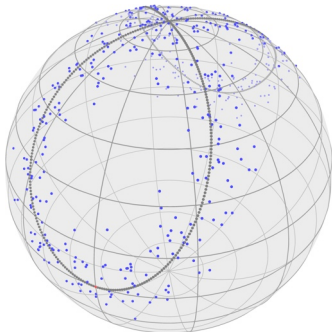
- comparison of f_0 & f_n with f_3
- denoising TV_1 & TV_2 ($\alpha = \frac{1}{2}, \beta = 1$)
- smallest mean squared error

Bernoulli's Lemniscate on the Sphere \mathbb{S}^2

$$\gamma(t) := \frac{a\sqrt{2}}{\sin^2(t) + 1} (\cos(t), \cos 1 \sin(t))^T, \quad t \in [0, 2\pi], a = \frac{\pi}{2\sqrt{2}}.$$

Generate a **sphere-valued signal** by putting it into the tangential plane of the north pole

$$\gamma_{\mathbb{S}}(t) = \log_p(\gamma(t)), p = (0, 0, 1)^T$$



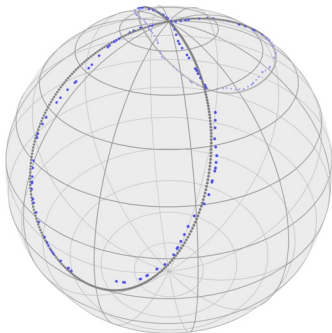
noisy lemniscate of Bernoulli on \mathbb{S}^2 , Gaussian noise, $\sigma = \frac{\pi}{30}$, on $T_p\mathbb{S}^2$.

Bernoulli's Lemniscate on the Sphere \mathbb{S}^2

$$\gamma(t) := \frac{a\sqrt{2}}{\sin^2(t) + 1} (\cos(t), \cos 1 \sin(t))^T, \quad t \in [0, 2\pi], a = \frac{\pi}{2\sqrt{2}}.$$

Generate a **sphere-valued signal** by putting it into the tangential plane of the north pole

$$\gamma_S(t) = \log_p(\gamma(t)), p = (0, 0, 1)^T$$



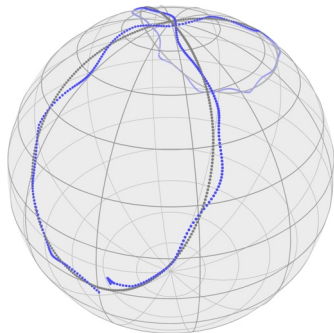
reconstruction with TV_1 , $\alpha = 0.21$, $MAE = 4.08 \times 10^{-2}$.

Bernoulli's Lemniscate on the Sphere \mathbb{S}^2

$$\gamma(t) := \frac{a\sqrt{2}}{\sin^2(t) + 1} (\cos(t), \cos 1 \sin(t))^T, \quad t \in [0, 2\pi], a = \frac{\pi}{2\sqrt{2}}.$$

Generate a **sphere-valued signal** by putting it into the tangential plane of the north pole

$$\gamma_S(t) = \log_p(\gamma(t)), p = (0, 0, 1)^T$$



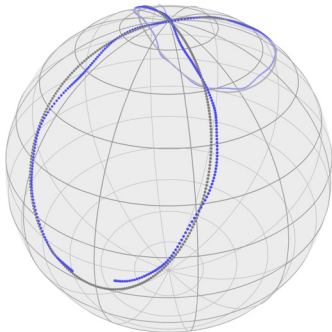
reconstruction with TV_2 , $\alpha = 0$, $\beta = 10$, $MAE = 3.66 \times 10^{-2}$.

Bernoulli's Lemniscate on the Sphere \mathbb{S}^2

$$\gamma(t) := \frac{a\sqrt{2}}{\sin^2(t) + 1} (\cos(t), \cos 1 \sin(t))^T, \quad t \in [0, 2\pi], a = \frac{\pi}{2\sqrt{2}}.$$

Generate a **sphere-valued signal** by putting it into the tangential plane of the north pole

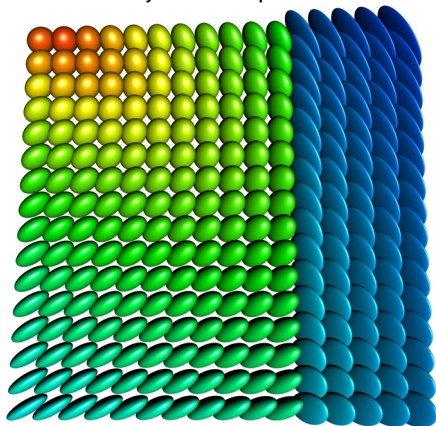
$$\gamma_S(t) = \log_p(\gamma(t)), p = (0, 0, 1)^T$$



reconstruction with TV_1 & TV_2 , $\alpha = 0.16$, $\beta = 12.4$, $MAE = 3.27 \times 10^{-2}$.

Inpainting of $\mathcal{P}(3)$ valued Images

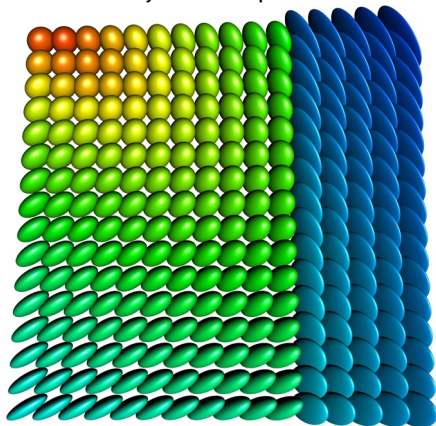
Illustrate symmetric positive definite 3×3 matrices as ellipsoids



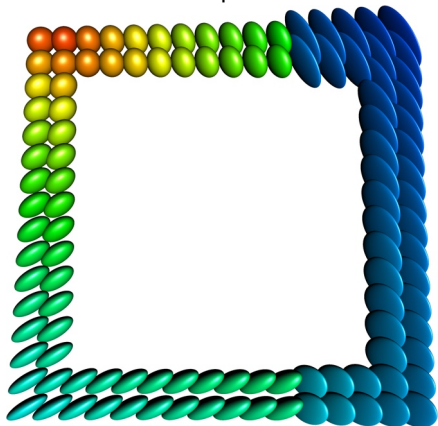
original data

Inpainting of $\mathcal{P}(3)$ valued Images

Illustrate symmetric positive definite 3×3 matrices as ellipsoids



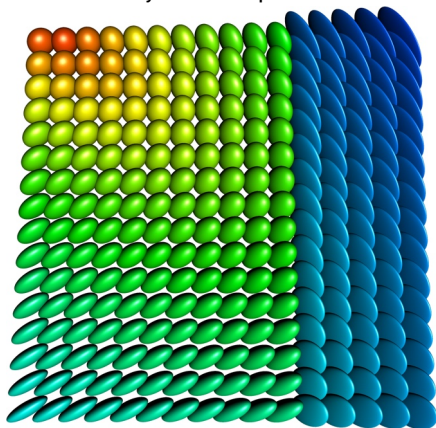
original data



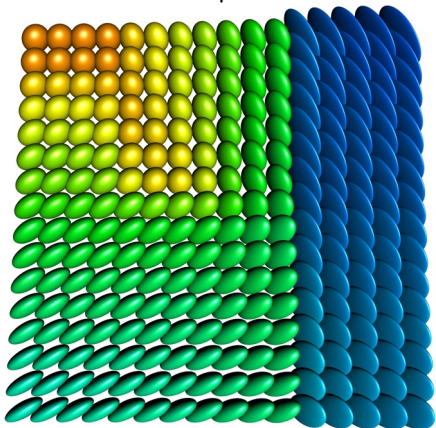
lost (a lot of) data

Inpainting of $\mathcal{P}(3)$ valued Images

Illustrate symmetric positive definite 3×3 matrices as ellipsoids



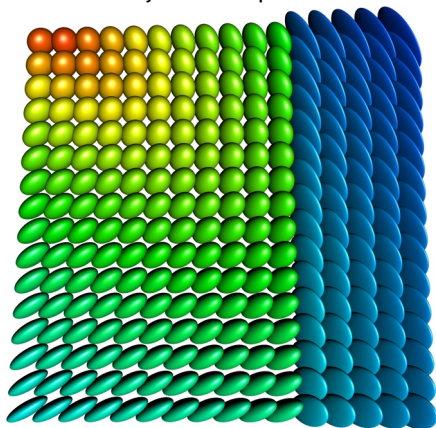
original data



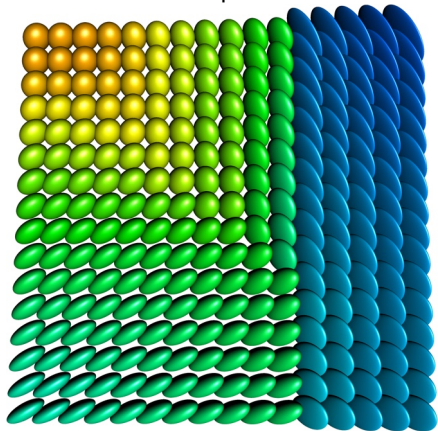
inpainted with $\alpha = \beta = 0.05$,
MAE = 0.0929

Inpainting of $\mathcal{P}(3)$ valued Images

Illustrate symmetric positive definite 3×3 matrices as ellipsoids



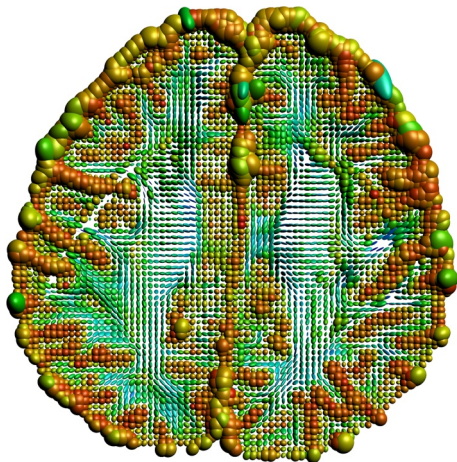
original data



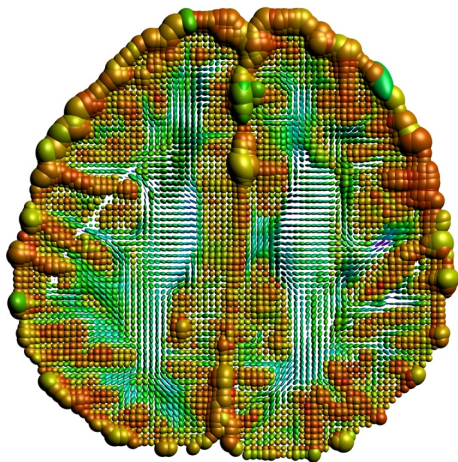
inpainted with $\alpha = 0.1$,
MAE = 0.0712

Diffusion Tensor Magnetic Resonance Imaging

Dataset $\mathcal{P}(3)^{112 \times 112 \times 50}$ of the human head, traversal plane $z = 28$



original data,

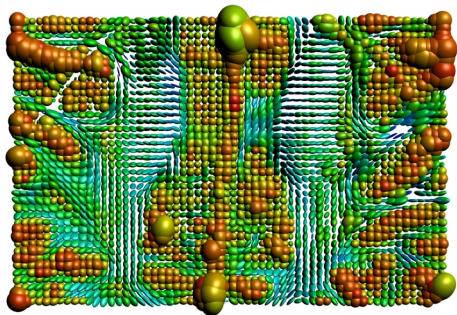


denoised, $\alpha = 0.01$, $\beta = 0.05$

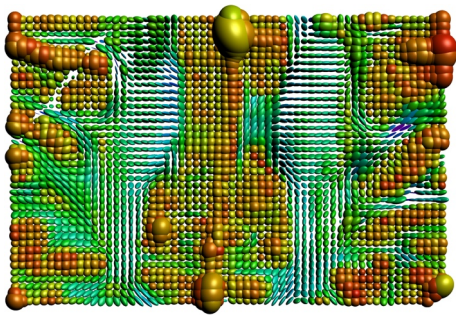
(Data available from The Camino Project, cmic.cs.ucl.ac.uk/camino)

Diffusion Tensor Magnetic Resonance Imaging

Dataset $\mathcal{P}(3)^{112 \times 112 \times 50}$ of the human head, traversal plane $z = 28$



original data,



denoised, $\alpha = 0.01$, $\beta = 0.05$

(Data available from The Camino Project, cmic.cs.ucl.ac.uk/camino)

a detail

- 1 Introduction
- 2 Second Order Differences on Manifolds
- 3 Proximal Mappings and the Cyclic Proximal Point Algorithm
- 4 Examples
- 5 Conclusion**

Conclusion

We have for manifold valued images $f: \mathcal{V} \rightarrow \mathcal{M}$

- a model for second order differences
- a first and second order TV-type functional $\mathcal{E}(u)$
- cyclic proximal point algorithm to minimize the functional $\mathcal{E}(u)$
- computed the proximal mappings using Jacobi fields
- proof of convergence
- examples of denoising and inpainting for manifold valued data

Future work

- an isotropic second order TV
- other couplings
- other algorithms

Literature

- [1] M. Bačák, R. Bergmann, G. Steidl, and A. Weinmann. A second order non-smooth variational model for restoring manifold-valued images. *Preprint, ArXiv #1506.02409*, 2015.
- [2] R. Bergmann, F. Laus, G. Steidl, and A. Weinmann. Second order differences of cyclic data and applications in variational denoising. *SIAM J. Imaging Sci.*, 2014.
- [3] R. Bergmann and A. Weinmann. A second order TV-type approach for inpainting and denoising higher dimensional combined cyclic and vector space data. *Preprint, ArXiv #1501.02684*, 2015.
- [4] J. Lellmann, E. Strelakovsky, S. Koetter, and D. Cremers. Total variation regularization for functions with values in a manifold. *IEEE ICCV*, 2013.
- [5] A. Weinmann, L. Demaret, and M. Storath. Total variation regularization for manifold-valued data. *SIAM J. Imaging Sci.*, 2014.

Literature

- [1] M. Bačák, R. Bergmann, G. Steidl, and A. Weinmann. [A second order non-smooth variational model for restoring manifold-valued images](#). *Preprint, ArXiv #1506.02409*, 2015.
- [2] R. Bergmann, F. Laus, G. Steidl, and A. Weinmann. [Second order differences of cyclic data and applications in variational denoising](#). *SIAM J. Imaging Sci.*, 2014.
- [3] R. Bergmann and A. Weinmann. [A second order TV-type approach for inpainting and denoising higher dimensional combined cyclic and vector space data](#). *Preprint, ArXiv #1501.02684*, 2015.
- [4] J. Lellmann, E. Strelakoskiy, S. Koetter, and D. Cremers. [Total variation regularization for functions with values in a manifold](#). *IEEE ICCV*, 2013.
- [5] A. Weinmann, L. Demaret, and M. Storath. [Total variation regularization for manifold-valued data](#). *SIAM J. Imaging Sci.*, 2014.

Thank you for your attention.